

# **Aplanatic grazing incidence diffraction grating: a new optical element**

Michael C. Hettrick

Applied Optics Vol. 25, Issue 18, pp. 3269-3282 (1986)

<http://dx.doi.org/10.1364/AO.25.003269>

© 1986 Optical Society of America. One print or electronic copy may be made for personal use only. Systematic reproduction and distribution, duplication of any material in this paper for a fee or for commercial purposes, or modifications of the content of this paper are prohibited.

# Aplanatic grazing incidence diffraction grating: a new optical element

Michael C. Hettrick

We present the theory of a grazing incidence reflection grating capable of imaging at submicron resolution. The optic is mechanically ruled on a spherical or cylindrical surface with varied groove spacings, delivering diffraction-limited response and a wide field of view at a selected wavelength. Geometrical aberrations are calculated on the basis of Fermat's principle, revealing significant improvements over a grazing incidence mirror. Aplanatic and quasi-aplanatic versions of the grating have applications in both imaging and scanning microscopes, microprobes, collimators, and telescopes. A 2-D crossed system of such gratings, similar to the grazing incidence mirror geometry of Kirkpatrick and Baez, could potentially provide spatial resolutions of  $\sim 200 \text{ \AA}$ .

## I. Introduction

Currently, there is significant interest in soft x-ray imaging below spatial dimensions of  $1 \text{ }\mu\text{m}$ . Instrumentally, this has been approached primarily through development of normal incidence optics, most notably in the use of transmission zone plates. Dramatic results have been obtained with this technique, including the imaging of living cells at a resolution of  $0.05 \text{ }\mu\text{m}$  using  $45\text{-\AA}$  synchrotron radiation.<sup>1</sup> In addition to biological microscopy, submicron imaging of x rays is of fundamental importance in other disciplines, including laser-produced plasmas,<sup>2</sup> microlithography,<sup>3</sup> and the materials sciences.<sup>4</sup> These applications represent the most challenging task yet requested of x-ray optical instrumentation.

Alternatives to the zone plate have so far been limited to mirror systems including multilayer coated normal incidence Schwarzschild objectives,<sup>5</sup> the grazing incidence axisymmetric mirror systems of Wolter,<sup>6-8</sup> and the crossed mirror system of Kirkpatrick and Baez.<sup>9</sup> Each of these approaches involves an unusual requirement on either the surface roughness, figure, system coalignment, or focal surface. The best spatial resolution yet obtained with any of these techniques has been  $\sim 1 \text{ }\mu\text{m}$ . An ideal optic to overcome these barriers would be spherical (permitting a high-quality

surface), operating at grazing incidence, focusing separately in each dimension (thus not require accurate coalignment), imaging onto a normal incidence focal surface, and free of the geometrical aberrations which have historically plagued grazing incidence optics.

Reflection gratings offer several potential advantages in this arena. They can be fabricated with large apertures (several  $\times 10^2 \text{ mm}$ ), allowing their use at grazing incidence. This provides for high-reflection efficiency and requires only modest groove densities compared to normal incidence mountings. Grazing incidence is also of practical significance in spreading high-intensity radiation and its associated heat load over a large geometric aperture. Reflection gratings can be easily formed on curved surfaces providing inherent imaging capability. Finally, unlike mirrors, grating imaging is also influenced by the presence of finite-order diffraction, allowing an extra degree of freedom which is crucial for aberration correction at the submicron level.

Diffraction gratings with groove spacings which vary in a continuous manner across the ruled width have been invoked in an increased number of situations for the purpose of aberration correction.<sup>10-14</sup> The most marked improvements have been obtained at grazing incidence, where mechanically ruled varied space gratings have been used to obtain normal incidence focal surfaces<sup>15</sup> and quasi-stigmatic soft x-ray images.<sup>16</sup> To date, these applications have been exclusively spectroscopic in nature and have not attempted to deliver spatial resolutions better than  $\sim 10 \text{ }\mu\text{m}$ .

We have recently determined that varied spacing can also be exploited to obtain a usable field of view for spatial imaging of an extended object at a specified wavelength. In addition, we intend to show that such

The author is with Lawrence Berkeley Laboratory, Center for X-Ray Optics, Berkeley, California 94720.

Received 24 March 1986.

0003-6935/86/183269-14\$02.00/0.

© Optical Society of America.

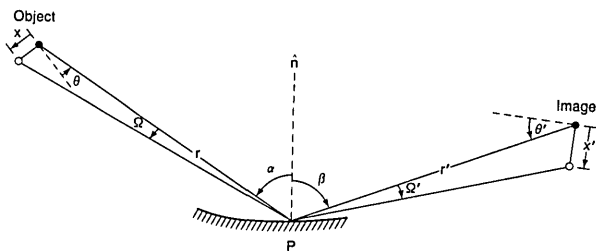


Fig. 1. Linear magnification of a diffraction grating at point  $P$  along its ruled width. The magnification  $M \equiv x'/x$  depends on the object and image distances, the incidence and diffraction angles, and the orientation of the focal planes. At grazing incidence, the magnification is largely influenced by the ratio  $\cos\beta/\cos\alpha$ , as illustrated.

a grating would provide spatial resolutions finer by a factor of several hundred than previously obtained with soft x-ray reflection gratings. In Sec. II, we introduce this new application and present an intuitive solution for the grating at unit magnification. Section III extends these principles to nonunit magnification, and in Sec. IV we develop 2-D imaging systems based on this optic. We conclude in Sec. V with a brief discussion of future directions for this work.

## II. Grating Imaging

### A. Aplanatism

The merit of an imaging system (e.g., a microscope or telescope) is based on two primary requirements: (1) stigmatism, i.e., pointlike, imaging between a particular object-image pair; and (2) uniform magnification independent of where a ray strikes the optical aperture. The famous sine rule of Abbe<sup>17</sup> states that a nearly uniform magnification is obtained if the ratio in sines of the incident and reflected angles, made with the axis joining object and image, is constant across the mirror aperture. This is equivalently stated as requiring a fixed image/object distance ratio ( $r'/r$ ) resulting in focal planes oriented normal to the optical axis. Given both stigmatism and a modified sine rule,<sup>18</sup> ray aberrations at the focal plane will grow only as second and higher powers of the off-axis field angle. Such optical systems are said to be aplanatic.

However, the sine rule does not apply to diffraction gratings. By differentiating the grating equation, one finds that the linear magnification depends not only on the image and object distances but also on the ratio in cosines of the incident/diffracted angles made with the local grating normal. At grazing incidence, this additional factor is significant, accounting for the familiar result that the magnification at the pole of a Rowland circle grating is unity despite a large inequity between the object and image distances. At grazing incidence, of course, the magnification varies in large amounts across the ruled width of this conventional optic, leading to a strong violation of aplanatism. The resulting field of view for spatial imaging is virtually unusable except along an oblique focal surface.

In place of the sine rule, a new trigonometric relationship governs the imaging behavior of diffraction gratings (see Fig. 1):

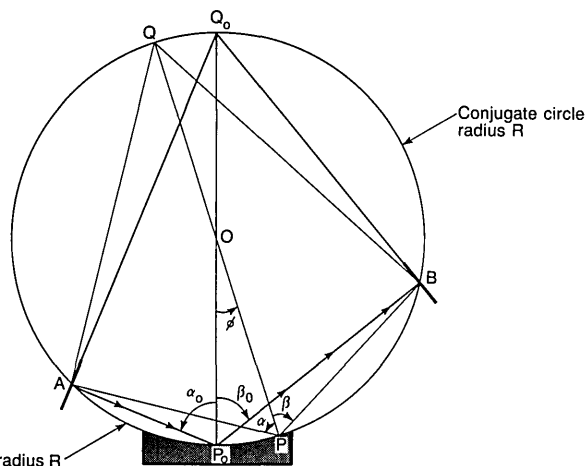


Fig. 2. Geometry of an aplanatic grating at unit magnification. The object  $A$  and image  $B$  lie along a circle which includes the surface of radius  $R$ . Inscribed right triangles  $APQ$  and  $BPQ$  share a common hypotenuse equal to the diameter of grating curvature. This results in a constant linear magnification independent of  $P$ . The focal surfaces are perpendicular to the principal ray (arrows).

$$M = (r'/r) \cdot (\cos\alpha/\cos\beta) \cdot (\cos\theta/\cos\theta'). \quad (1)$$

In this equation,  $M$  is the linear magnification,  $r$  is the object distance,  $r'$  is the image distance,  $\alpha$  is the angle of incidence,  $\beta$  is the angle of diffraction,  $\theta$  is the ray angle made with the object plane, and  $\theta'$  is the ray angle made with the image plane. The first factor ( $r'/r$ ) accounts for the classical sine rule, and the second factor ( $\cos\alpha/\cos\beta$ ) provides the effect of grating diffraction when used in a finite spectral order. The last factor ( $\cos\theta/\cos\theta'$ ) is approximately unity for normal incidence focal surfaces ( $\theta_0 = \theta'_0 = 0$ ), representing an obliquity correction to the magnification.

We first seek to obtain 1-D solutions for the optical surface shape along which the magnification  $M$  is constant. In general, this is an ungratifying mathematical exercise, as Eq. (1) contains quantities which are defined in three different coordinate systems (fixed, relative to the grating surface, and relative to the focal surface). Before attacking this problem directly, we first gain some physical insight by considering unit magnification. In this case, the included angle of the light beam (i.e., its numerical aperture) is equal at the object and image planes. Thus  $\theta(w) = \theta'(w)$ , where  $w$  is the ruled width coordinate, yielding a constant obliquity factor of unity. Equation (1), therefore, reduces to the equality  $r'/\cos\beta = r/\cos\alpha$ , permitting a simple geometrical construction as shown in Fig. 2. The object and image lie along a conjugate focal surface which includes a circular grating surface of radius  $R$ . The conjugate surface is thus twice the radius of the classical Rowland circle. In the grazing incidence limit (incidence or diffraction angle tending toward  $90^\circ$ ), the respective focal distance vanishes as the cosine of the incidence (or diffraction) angle, thus maintaining a uniform grating magnification.

## B. Varied Spacing

Of course, a conventionally ruled grating, having equidistant grooves, will not focus in this manner. Stigmatism at wavelength  $\lambda$  between the object point  $A$  and image point  $B$  requires a smooth variation in the groove spacing  $\sigma$  as a function of the ruled width coordinate  $w$ :

$$\sigma(\Phi) = m\lambda_* / [\sin\beta(\Phi) - \sin\alpha(\Phi)], \quad (2a)$$

where

$$\alpha(\Phi) = \alpha_0 - \Phi/2 \text{ and } \beta(\Phi) = \beta_0 + \Phi/2 \quad (2b)$$

are the local angles of incidence and diffraction and where  $\Phi = \arcsin(w/R)$  is the angular position of the groove relative to a polar coordinate system (Fig. 2). At the grating pole ( $\Phi = 0$ ) all quantities are ascribed subscripts 0. If we set  $\beta_0 = \alpha_0 \equiv \pi - \gamma_0$ , the groove spacing is

$$\sigma(\Phi) = m\lambda_* / \sin\gamma_0 / 2 / \sin(\Phi/2), \quad (2c)$$

where  $\gamma_0$  is the graze angle, and  $m$  and  $\Phi$  have the same sign. To a high degree of accuracy, the groove density is thus linearly proportional to the aperture coordinate  $\Phi$ . The groove spacings are thus similar to, but a factor of  $2/\sin\gamma_0$  larger than, those of a transmission zone plate away from its symmetry axis.<sup>19,20</sup> The factor of 2 arises because there are two zones (one transparent plus one opaque or refractory) per groove. However, the most significant difference is due to the factor  $1/\sin\gamma_0$ , which represents the effective spacing of a groove as projected onto a plane normal to the line of sight. For example, at a graze angle of  $4^\circ$  the groove spacing is  $\sim 14\times$  larger than two corresponding zones of an equivalent focal length zone plate at normal incidence. This is of great practical significance, permitting fabrication of the present design by mechanical means. This contrast with the situation of fabricating a high-resolution zone plate.<sup>21,22</sup>

With such a space variation, object point  $A$  will be focused without aberration to image position  $B$ , and the focal surfaces for imaging of nearby points will be normal to the principal ray, as shown in Fig. 2. We note that these focal surfaces are for spatial imaging, to be distinguished in all regards from the spectral focal surface for imaging of  $A$  at wavelengths other than  $\lambda_*$ . Due to the variation in groove spacing, this focal surface is an unconventional curve (not the Rowland circle) of little interest in the present context and is not shown in Fig. 2.

From Eq. (2), it is evident that the groove spacing becomes infinite at the grating coordinate  $\Phi = (\alpha_0 - \beta_0)$ , where the angles of incidence and diffraction are equal. This equality is usually associated only with zero-order (mirror) reflection. However, in the present situation this interpretation is not valid. The varied groove spacings maintain a change in path length of the rays equal to  $m\lambda_*$  between successive grooves. Thus the grating operates in finite order across its entire ruled width. It should be recognized that, although  $\sigma$  can become locally infinite, the distance to adjacent grooves is always finite. This is

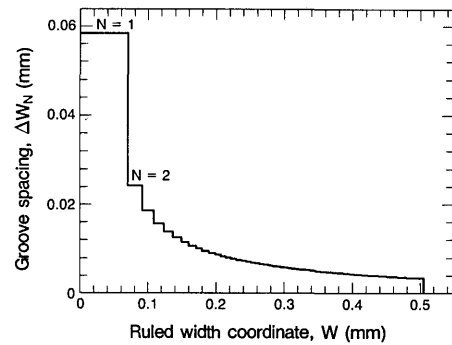


Fig. 3. Spacings between grooves near the center of an aplanatic grating. The radius of curvature is 50 mm, is aplanatic at  $45 \text{ \AA}$  in unit magnification, and is operated at incidence and diffraction angles both equal to  $82^\circ$  at the grating pole ( $w = 0$ ). For groove number  $N \gg 1$ , the spacing is inversely proportional to  $w$ .

understood by writing the equation for the groove number  $N$ :

$$mN\lambda_* = \sqrt{(r_0 \sin\alpha_0 + w)^2 + [r_0 \cos\alpha_0 - (R - \sqrt{R^2 - w^2})]^2} - r_0 + \sqrt{(r'_0 \sin\beta_0 - w)^2 + [r'_0 \cos\beta_0 - (R - \sqrt{R^2 - w^2})]^2} - r'_0. \quad (2d)$$

In Fig. 3 we have plotted the actual distance between groove  $N - 1$  and  $N$ ,  $\Delta w_N$ , as a function of the distance away from the point at which the incidence and diffraction angles are equal ( $\alpha = \beta = 82.0^\circ$ ). The curvature radius  $R = 50 \text{ mm}$  and  $m\lambda_* = 45 \text{ \AA}$ . Because  $w$  is the linear coordinate along the grating basal plane, the groove spacing  $\sigma$  along the surface tangent is  $\Delta w_N / \cos(w/R)$ . A smooth curve fitted through this plot agrees with the results of Eq. (2c); however, the discreteness in spacing is evident at small ruled widths and results at the grating pole in a finite spacing of  $\sim 0.06 \text{ mm}$ . Nonetheless, this region would be avoided in practice during a mechanical ruling due to the associated impractical requirements of either a vanishing blaze angle or large groove depth at this location.

The selection of  $\alpha_0$  and  $\beta_0$  involves a number of considerations. The incidence angle must allow efficient reflection from the grating surface at the wavelength of use. In addition, the separation of the diffracted and incident angles determines the required number of grating grooves over a given ruled width. To deliver a diffraction width limited by the entire aperture size, each groove must provide a phase shift in the diffracted beam equal to  $m$  wavelengths relative to the adjacent groove. To prevent chromatic aberrations, the incident light must be coherent over the net phase shift across the grating. The net spectral resolution required of the beam is

$$\lambda/\Delta\lambda = R \int_{\Phi_a}^{\Phi_b} m \cdot d\Phi/\sigma(\Phi), \quad (3a)$$

where  $m$  changes sign at  $\Phi = \alpha_0 - \beta_0$  and where  $\Phi_a$  and  $\Phi_b$  lie on the range  $\Phi_{\min}$  to  $\Phi_{\max}$  and are chosen to find the largest value of  $\lambda/\Delta\lambda$ . The numerical aperture  $a = (\Phi_{\max} - \Phi_{\min})/2$  for the unit magnification aplanatic

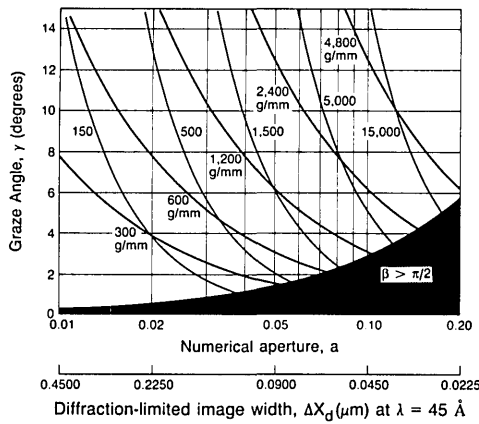


Fig. 4. Curves of constant groove density at grating edge (dark) and required monochromaticity of incident light in  $\lambda/\Delta\lambda$  (light) for unit magnification aplanatic grating. The wavelength is  $45 \text{ \AA}$ , and the radius of grating curvature is  $50 \text{ mm}$ . For magnifications small or large compared to unity, divide the groove densities indicated here by a factor of 2 and the values of  $\lambda/\Delta\lambda$  by a factor of 4.

grating, which is half of the value of a Rowland circle configuration. For the centered case,  $\alpha_0 = \beta_0$ , we have  $\Phi_a = 0$ ,  $\Phi_b = \Phi_{\max}$ , and the required spectral resolution is minimized. Combining Eqs. (2c) and (3a), we have

$$\begin{aligned} \lambda/\Delta\lambda &= a^2 R \sin\gamma_0 / (2\lambda) \\ &= \lambda_* R \sin\gamma_0 / (2\Delta x_d^2), \end{aligned} \quad (3b)$$

where  $\Delta x_d = \lambda_*/a$  is the diffraction-limited image width for a filled rectangular aperture. Given a continuum light source, or one with a bandpass  $>\Delta\lambda$ , this requires use of a premonochromator. Even if it could be made 100% efficient, the transmitted throughput would decrease linearly with  $\Delta\lambda$ . It is thus of practical advantage to minimize  $\lambda/\Delta\lambda$ . Immediately evident is that a small curvature radius  $R$  is required. For example, consider the use of  $45\text{-\AA}$  radiation to obtain a diffraction spot of  $900\text{-\AA}$  ( $0.09\text{-}\mu\text{m}$ ) extent. On the basis of physical optics, this requires a numerical aperture  $a \geq 0.05$ . Furthermore, to obtain 20% reflection from a coated (e.g., osmium) surface at this wavelength requires a grazing angle  $\gamma_0$  of  $\sim 8^\circ$ .<sup>23</sup> Equation (3b) then reveals that a  $50\text{-mm}$  curvature (the smallest commercially available) requires a spectral resolution of 2000. In practice, this coherency requirement may be conservative, as wavelengths other than  $\lambda_*$  will be focused poorly on the chosen image plane and thus result in less degradation of the FWHM (full width at half maximum) image than the extremum width given by Eq. (3b). The grating would have a ruled width of  $5 \text{ mm}$  at the edges of which the groove density would rise to  $\sim 1600 \text{ g/mm}$ .

In Fig. 4 we plot the grating parameters  $\gamma_0$  and  $a$  for various values of the required spectral resolution and groove density at the grating edge for a grating curvature radius of  $50 \text{ mm}$ . The groove densities assume use of the first spectral order, and the required spectral resolution and lower horizontal scale (diffraction-limited resolution) assume  $45\text{-\AA}$  radiation. The unallowed region of parameter space corresponds to grat-

ings so large they would extend through the object and image points, where the grating efficiency vanishes due to the incident or diffracted ray lying along the surface tangent. Given the availability of quasi-stigmatic high-resolution ( $\lambda/\Delta\lambda \approx 10^4$ ) soft x-ray monochromators<sup>24,25</sup> and sufficiently intense soft x-ray light sources,<sup>26</sup> it is evident from this graph that spatial resolutions in the  $0.05\text{--}0.10\text{-}\mu\text{m}$  range are accessible.

The diffraction-limited spatial resolution improves linearly as the wavelength is shortened. For example, at  $\lambda_* = 8 \text{ \AA}$ , a numerical aperture of only 0.02 would permit a resolution of  $0.04 \text{ }\mu\text{m}$ . Efficient reflection at this wavelength would require a graze angle of  $\sim 1.5^\circ$  or a factor of  $\sim 5$  smaller than at a wavelength of  $45 \text{ \AA}$ . From Eqs. (2c) and (3b), we see that the effect of a graze angle which decreases linearly with the wavelength results in an unchanged groove density and spectral resolution for a fixed numerical aperture. From Fig. 4, we therefore infer the requirements of  $600 \text{ g/mm}$  and  $\lambda/\Delta\lambda = 300$ , representing a relaxation over those at longer wavelengths for the same spatial resolution.

### C. Geometrical Aberrations

Of fundamental importance is the effective field of view for imaging of a finite size object centered at point A. The size of this field is set by the off-axis grating aberrations. We shall employ Fermat's principle,<sup>17</sup> which requires that a light ray will trace a path in the image plane which maintains a stationary optical path length (phase) locally across the ruled width:

$$x(w) = r'(w) \cdot dF(w)/dw / \cos\beta(w), \quad (4)$$

where  $x$  is the image position in the direction of grating dispersion. Along our aplanatic conjugate circle we have  $r'(w) = 2R \cos\beta(w)$  exactly. Thus  $x(w) = 2R dF(w)/dw$ . In passing, we note that this cancellation of the dependence on  $w$  is not exact in the classical derivation of image aberrations for the Rowland circle.

The light path function  $F(w)$  for a spherical grating is well known.<sup>27,28</sup> Given stigmatism at the fixed wavelength  $\lambda_*$ , as provided by mechanical ruling following Eq. (2), the aberrant light path function over a finite field of view can be written simply as the difference in path length traveled in going from the off-axis object and image points. As a power series in the grating coordinates  $(w, l)$ ,

$$F(w) = \sum_{ij} [F_{ij}(\alpha, \beta, r, r') - F_{ij}(\alpha_0, \beta_0, r_0, r'_0)] w^i l^j, \quad (5a)$$

where the lowest-order aberration coefficients  $F_{i0}$  are

$$F_{20} = \frac{1}{2}(\cos^2\alpha/r - \cos\alpha/R) + \frac{1}{2}(\cos^2\beta/r' - \cos\beta/R), \quad (5b)$$

$$\begin{aligned} F_{30} &= -\frac{1}{2}(\sin\alpha/r)(\cos^2\alpha/r - \cos\alpha/R) \\ &\quad + \frac{1}{2}(\sin\beta/r')(\cos^2\beta/r' - \cos\beta/R), \end{aligned} \quad (5c)$$

$$\begin{aligned} F_{40} &= \frac{1}{2}[(\sin^2\alpha/r^2)(\cos^2\alpha/r - \cos\alpha/R) \\ &\quad - \frac{1}{4}(\cos^2\alpha/r - \cos\alpha/R)^2/r + \frac{1}{4}(1/r - \cos\alpha/R)/R^2 \\ &\quad + (\sin^2\beta/r'^2)(\cos^2\beta/r' - \cos\beta/R) \\ &\quad - \frac{1}{4}(\cos^2\beta/r' - \cos\beta/R)^2/r' \\ &\quad + \frac{1}{4}(1/r' - \cos\beta/R)/R^2]. \end{aligned} \quad (5d)$$

The omission of terms in Eqs. (5b)–(5d) which depend on the groove spacing is justified by the fact that these would cancel in forming the subtraction of Eq. (5a). We note that terms in the groove length  $l$  have not been included here, as this analysis is restricted to the ruled width dimension. Adopting flat focal surfaces normal to the principal (on-axis) ray, we have used Eqs. (4)–(5) to generate image envelopes for off-axis point sources:  $\alpha = \alpha_0 + \Omega$ ;  $\beta = \beta_0 + \Omega (\cos\alpha_0/\cos\beta_0)$ . We plot in Fig. 5 the geometric aberrations of the unit magnification grating introduced above as a function of off-axis field angle  $\Omega$ . The quadratic growth in the image size with field angle verifies the aplanatic nature of this grating. A resolution of  $0.1 \mu\text{m}$  is achieved over a field of view of  $\pm 10 \mu\text{m}$ , which indicates its potential for imaging of extended objects. This result has been confirmed by preliminary ray tracings.<sup>29</sup>

For comparison, we have also plotted in Fig. 5 the results for a spherical mirror having the same numerical aperture, graze angle, and radius of curvature as the aplanatic grating. Although the physical optics limit is the same ( $0.09 \mu\text{m}$ ), spherical aberration limits the mirror to resolutions of the order of  $10 \mu\text{m}$ . Even if this term were to vanish by use of an ellipse figured to the required accuracy (in practice representing a significant advance in the technology of mirror fabrication), the defocusing term  $x_{20}$  would be unchanged. Its linear growth with off-axis angle would limit the field of view to approximately one resolution element. This can be remedied only by use of an oblique focal surface, for which detection efficiencies are generally small. One, therefore, gains dramatic practical improvement (a factor of  $\sim 100$ ) in imaging through use of a diffraction grating.

#### D. Optical Aperture Limit

The physical diffraction limit included in the above analysis assumes comparable efficiency from all parts of the grating aperture. In practice, this is complicated by the potentially large variation in blaze efficiency across the width of a ruled concave grating.<sup>30,31</sup> This can be understood by considering the shift in the classically blazed wavelength, which can be expressed analytically (see Fig. 5):

$$m_B \lambda_B(\Phi) / m \lambda_c = 2 \sin \delta \sin \gamma / (\sin \beta - \sin \alpha), \quad (6)$$

where the incidence angle  $\alpha$ , diffraction angle  $\beta$ , facet graze angle  $\gamma$ , and the blaze angle  $\delta$  all vary as functions of the ruled width. The variations in  $\alpha$  and  $\beta$  are taken from Eq. (2b), and the facet graze angle is

$$\gamma = \pi/2 - \alpha_0 + \Phi/2 - \delta(\Phi). \quad (7)$$

The variation in blaze angle is of prime importance. From a theoretical point of view, the optimal ruling geometry would provide a rotation of the tool orientation as a function of the ruled width. From Eq. (6a), one derives that a half-speed rotation ( $\Phi/2$ ) would maintain a constant blazed wavelength equal to the stigmatic wavelength. As the angular deviation ( $\alpha + \beta$ ) is fixed across the unit magnification aplanatic grat-

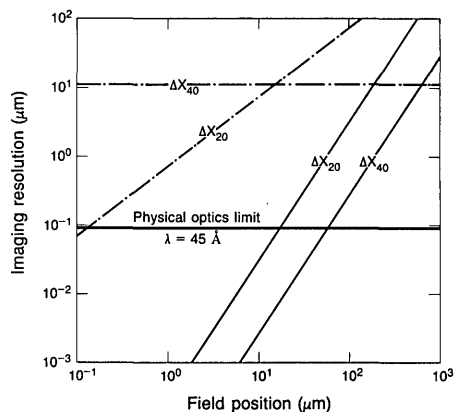


Fig. 5. Geometrical extremum aberrations vs off-axis position of a field point. Optical surface has a radius of curvature of 50 mm, subtends a numerical aperture of 0.05, and is operated at unit magnification with incidence and diffraction angles equal to  $82^\circ$ . Solid lines are for the aplanatic grating, and dot-dash lines are for a conventional mirror. The aplanatic grating is absence of linear field aberrations. The two subscripts refer to the powers in ruled width and groove length, respectively, on which the wave aberration grows.

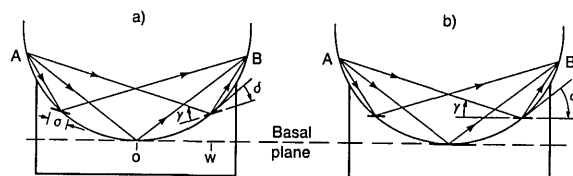


Fig. 6. Orientation of groove facets for aplanatic grating at unit magnification: (a) a rotation of the facets as a function of ruled width results in uniform blazing at the desired wavelength; (b) more common condition of a fixed facet orientation relative to the basal plane.

ing, this blazing would also maintain a constant graze angle on the facets and a constant groove depth. Such an ideal geometry is pictured in Fig. 5. From the practical point of view, however, this would be challenging. While multipartite concave gratings are commonly ruled with multiple settings of blaze angle across the ruled width,<sup>32</sup> the phase coherence between different panels is almost certainly lost. In the present design, this would be unacceptable due to the need for a diffraction-limited full aperture. Therefore, the ruling must provide either for means of continuous change of the blaze angle or for monitoring of the diamond tip position during reorientation of the blaze angle at discrete intervals along the ruled width. In the above example, the blaze angle would need to change by  $\sim 3^\circ$  in total across the 5-mm ruling.

In the circumstance of a fixed diamond orientation [Fig. 6(b)], we have

$$\delta(\Phi) = \delta_0 + \Phi, \quad (8)$$

where perfect blazing at  $\Phi = 0$  requires  $\delta_0 = (\beta_0 - \alpha_0)/2$ . Using Eqs. (6)–(8), we have plotted in Fig. 7 the ratio of the blazed wavelength to stigmatic wavelength for the mounting  $\alpha_0 = 84^\circ$ ,  $\beta_0 = 80^\circ$ , and  $\delta_0 = -2^\circ$ . This curve exhibits two anomalies, which are associated with (1) a large groove spacing and (2) a vanishing blaze angle, at different points along the ruled width. If one blazed

$\alpha_0 = \beta_0$ , these two effects would coincide and produce the curious result of a blazed wavelength equal to twice the stigmatic wavelength independent of the spectral order. Even in first order, this would lead to an efficiency near zero. Avoiding these anomalies and requiring a blazed wavelength within a factor of 2 from the wavelength of use, the usable numerical aperture is only 0.05 or marginally consistent with the assumed diffraction limit of 0.09- $\mu\text{m}$  resolution in Sec. II.C.

### III. Nonunit Magnification

Practical attainment of submicron resolution is facilitated in many cases if the system can be designed with high magnification ( $M \sim 100$ ). This provides convenient coupling with high-efficiency film<sup>33,34</sup> and electronic detectors<sup>35</sup> or permits demagnification of laboratory microfocus light sources<sup>36</sup> from 10- $\mu\text{m}$  spatial extents to the desired microprobe size of  $<0.1 \mu\text{m}$ . The analytic exercise presented in Sec. II serves as an introduction to the essential principles on which this new optic is based. In this section, we apply these principles to the construction of an aplanatic grating with the desired high magnification. In this case, the desired aplanatic geometry is not as evident as it was for unit magnification. In Secs. II.A and B, we present two approaches for the derivation of these grating surfaces.

#### A. General Differential Equation

Recognizing aplanatism as the condition for which the linear magnification  $M$  is constant over the optical aperture, we proceed to generate the general surface equation for which this is true. Adopting a Cartesian coordinate system  $(x,y)$  with object point at  $(0,-1)$  and image point at  $(0,+1)$ , the trigonometric rule given in Eq. (1) can be written as

$$M \cdot \frac{[x^2 + (1+y)^2]}{[x^2 + (1-y)^2]} = \frac{[xy' - (1+y)]}{[xy' + (1-y)]}, \quad (9)$$

where  $y'$  is the surface slope and normal incidence focal surfaces ( $\theta_0 = \theta'_0 = 0$ ) are adopted. Even with this condition, Eq. (9) is an approximation as it neglects the small obliquity of these focal planes relative to rays not striking the grating center. These terms introduce ray aberrations dependent on the second power of the aperture.

In the case of  $M = 1$ , Eq. (9) reduces to that of a circle with arbitrary radius passing through the object and image points. This is the closed form solution previously inferred from intuitive arguments. However, in general we have a highly nonlinear differential equation which does not simplify to the form  $y = y(x)$ . At best, we can rewrite Eq. (9) in the form  $y' = y'(x)$ :

$$y' = \frac{(M-1)(y^2 + x^2 - 1)y + (M+1)(y^2 - x^2 - 1)}{x[(M-1)(y^2 + x^2 + 1) + 2(M+1)y]}, \quad (10)$$

which can be integrated by straightforward numerical methods.

We recognize from Eq. (1) that grazing incidence solutions must pass through both the object and image points so as to maintain a finite magnification in the

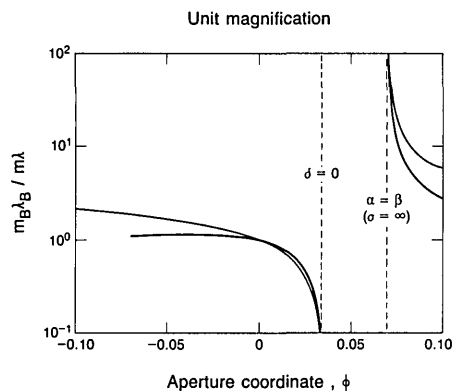


Fig. 7. Variation in blazed wavelength  $\lambda_B$  relative to the wavelength of use  $\lambda$  as a function of the ruled width across a unit magnification aplanatic grating. The incidence angle is  $84^\circ$ , the diffraction angle is  $80^\circ$ , and the grating facets are in a fixed orientation. Heavy curves correspond to a calculation based on an outside spectral order, and light curves are for an inside spectral order. The ratio  $\lambda_B/\lambda$  stays within the usable range of 0.5–2.0 over a numerical aperture of  $\sim 0.05$  ( $\Phi_{\max} - \Phi_{\min} = 0.1$ ).

limit as the incident or diffracted angle approaches  $\pi/2$ . However, so as not to constrain the solution by these intuitive arguments, we choose as the starting point for numerical integration the center of a grating for which  $\alpha_0 = \beta_0$ . The initial conditions can then be written

$$y'_0 = \tan(\pi - \alpha_0 - b), \quad (11a)$$

$$x_0 = r_0 \sin b, \quad y_0 = r_0 \cos b - 1, \quad (11b)$$

where

$$r_0 = 2/\sqrt{1 + M^2 - 2M \cos 2\alpha_0}, \quad (11c)$$

$$b = \arcsin \{M \sin 2\alpha_0 / \sqrt{[1 + M \cos^2(\pi - 2\alpha_0)]^2 + (M \sin 2\alpha_0)^2}\}. \quad (11d)$$

As initial values we set  $M = 3$  and, for clarity,  $\alpha_0 = 60^\circ$  and plot in Fig. 8 the results of an Euler method inte-

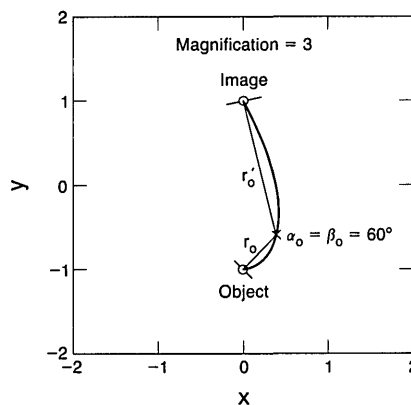


Fig. 8. Grating surface which is aplanatic for imaging at nonunit magnification. The focal surfaces are at normal incidence relative to the principal ray. For clarity, a magnification of 3 is shown, and the graze angle is  $30^\circ$  at the grating pole. The grating surface passes through both image and object. These results were obtained by numerical integration of the differential equation expressing aplanaticism in the case where the small obliquity of field for nonprincipal rays was ignored.

gration of Eq. (10). As predicted, the grating surface passes through both the object and image points where the numerical integration is interrupted. This result confirms a general characteristic of the aplanatic grating, which distinguishes it from both normal incidence zone plates and other grazing incidence optics.

## B. Characteristic Functions

However, the surface shape displayed in Fig. 8 for the case of nonunit magnification is clearly not circular. This is unfortunate as spherical surfaces can be figured with the high metrological accuracy required to form submicron images (representing wavefront errors less than  $\sim\lambda_*/4$  at grazing incidence). We, therefore, attempt to approximate the aplanatic surface by a circle with radius  $R$  and refer to this as a quasi-aplanatic grating.

A finite curvature radius permits removal of the linear growth in the first-order  $F_{20}$  aberration of Eq. (5b) (Sec. II.C). The correct focusing condition is obtained by differentiation of this term relative to the field angle  $\Omega$  of the object and that of the image  $\Omega' = \Omega \cos\alpha_0/\cos\beta_0$ , at a fixed wavelength. Given normal incidence focal planes, the object and image distances do not vary over the field to within the accuracy of these first-order calculations. Setting this differential equal to zero, we have the equation for quasi-aplanatic focusing:

$$\sin\alpha_0/r_0 + \sin\beta_0/r'_0 = \frac{1}{2}(\tan\alpha_0 + \tan\beta_0)/R. \quad (12a)$$

In terms of the magnification  $M$ , this yields the positions of object and image points given a fixed radius:

$$r_0 = 2R \cos\alpha_0(\tan\alpha_0 + \tan\beta_0/M)/(\tan\alpha_0 + \tan\beta_0); \quad (12b)$$

$$r'_0 = Mr_0 \cos\beta_0/\cos\alpha_0. \quad (12c)$$

In the case of unit magnification, these results confirm the radius previously given for a fully aplanatic grating:  $r_0 = 2R \cos\alpha_0$ ,  $r'_0 = 2R \cos\beta_0$ .

At high magnification, we see from Eq. (12b) that the object distance approaches  $R \cos\alpha_0$  for the case  $\beta_0 = \alpha_0$ , and the image distance tends toward infinity. The numerical aperture of the grating is, therefore, equal to the full angle subtended by the ruled width at the center of curvature. This is twice as large as obtained with unit magnification, allowing a smaller diffraction-limited image (or object). Thus Fig. 4, devised for the case of  $M = 1$ , can also be applied approximately to the case of large  $M$  by simply multiplying the groove densities by one-half and the required resolving powers by one-fourth. Similar modifications should be made in Eqs. (2c) and (3b). With this scaling, it is evident that numerical apertures as large as 0.2 are accessible on the basis of available monochromatic light sources and ruling densities.

While linear field aberrations are now absent from the dominant first-order aberration term, this approximation cannot simultaneously remove such linear growths in terms dependent on higher powers of the ruled width. To minimize the required groove density of the grating and coherency of the incident light, we

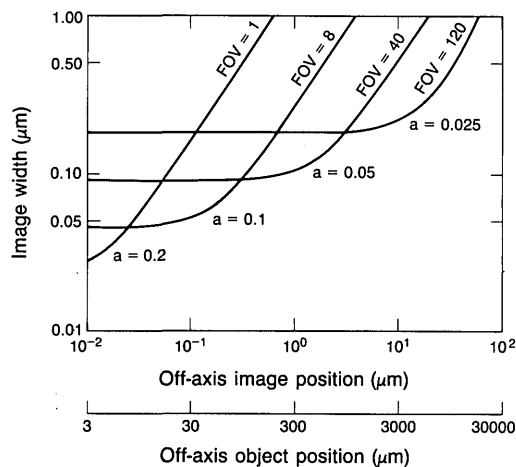


Fig. 9. Total image width vs field position for a quasi-aplanatic grating (constant radius) at a magnification of 1/300. The radius of curvature is 50 mm, the graze angle is  $8^\circ$ , and the wavelength is  $45 \text{ \AA}$ . Different numerical apertures are plotted, each reaching a lower limit set by the physical diffraction width. The encompassed number of pixels at that resolution limit is FOV. A resolution finer than  $\sim 0.1 \text{ \AA}$  is most suited to use in a scanning mode.

consider as before the case of a central mounting  $\beta_0 = \alpha_0$ . We set the magnification  $M = 300$ , and as before the curvature radius  $R = 50 \text{ mm}$  and the graze angle  $= 8^\circ$ . In Fig. 9, we plot the quadrature sum of all geometrical field aberrations, using the formalism developed in Sec. II.C, summing also the physical diffraction limit for values of the numerical aperture between  $a = 0.025$  and  $a = 0.2$ . Imaging at spatial resolutions of  $0.1 \text{ \AA}$  is shown to include  $\sim 50$  pixels within its field of view. For numerical apertures of less than  $\sim 0.1$ , third-order wave aberrations dominate, resulting in a number of pixels proportional to  $a^2$ . Thus, at a comparatively coarse resolution of  $1 \text{ \AA}$ , the field of view encompasses 2000 1-D pixels. However, at large numerical aperture, fourth-order aberrations quickly set it, limiting the field of view to less than one resolution element at  $0.03 \text{ \AA}$  ( $300 \text{ \AA}$ ). This precludes direct use for imaging of spatially extended objects; nonetheless, such a stigmatic grating would be ideal for use as a microprobe. Using a light source of extent of  $< 10 \text{ \AA}$  and positioned within  $5 \text{ \AA}$  of the optimal object position, a demagnification of 300 would deliver a  $300\text{-\AA}$  spot diameter. Such performance would be extremely useful as a scanning microscope.

Scanning microscopes using zone plates<sup>37</sup> require an aperture stop obscuration in the central region to minimize background due dominantly to zero-order contamination of the object.<sup>38</sup> In a blazed reflection grating scanning microscope of the type suggested above, the ratio of zero order to first-order efficiency is lower, and thus the requirement for such a stop is not as strong. Yet, an advantage of a stop at the grating center would be the relaxed coherency requirement on the beam as well as a reduced aberration. A balancing consideration is that such apodization results in comparatively more intense sidelobes of the diffraction-limited spot, an effect which has recently been discussed also for grazing incidence reflection gratings.<sup>39</sup>

The resolution plotted in Fig. 9 is somewhat conservative, because each aberration was treated independently and then added in modulus. However, one can obtain some improvement by deviating from the focusing Eq. (12) and thereby cancel the first-order and third-order ray aberrations at the grating edge. Combined with an aperture stop at the grating center, which would decrease the dominant second-order aberration, the field of view could be widened by  $\sim 100\%$ . Thus the results shown in Fig. 8 could be extended to  $\sim 200\text{-\AA}$  resolution. More substantial improvements would require independent removal of the linear field growth in the various higher-order aberrations. This requires invoking a noncircular surface in the direction of ruled width, leading to polynomial surface coefficients derived in a manner similar to Eq. (12). The ultimate result of that exercise would be convergence to a completely aplanatic grating surface, as plotted in Fig. 8. However, given the unavailability of acircular or aspherical surfaces figured or bent to the required high tolerances for this application, we do not develop these solutions further in this work.

### C. Infinite Magnification

As in the case of unit magnification, there are several practical considerations regarding the grating parameters for nonunit magnification. These include the variations required of the groove density and blaze angle and the resulting limits on the usable efficient grating aperture. For nonunit magnification, there are also unavoidable and undesired variations in the groove depth and grazing angle on the illuminated facets. In principle, one can appeal to the classical formalism, and expand all the grating parameters in powers of the ruled width coordinate  $w$ . However, the grating under consideration extends to very high numerical apertures (as large as 0.2) where the convergence of the power series is very slow. Rather than retaining the large number of terms one would need, we consider here the limiting case of infinite magnification (i.e., a telescope or collimator). In this limit, exact analytic solutions are easily expressed for all the important design parameters. Although the detailed values for these parameters will be different at some finite magnification, the general behavior of the solutions should not change provided the magnification is large (e.g.,  $M \sim 10$  or larger).

The geometry is shown in Fig. 10. An object lies along a circle of diameter equal to the radius of grating curvature  $R$  and is an object source of light (wavelength  $\lambda_*$ ) striking the grating pole ( $\Phi = 0$ ) at an incident angle  $\alpha_0$ . When provided with appropriate groove space variation, the grating diffracts the light into a collimated beam making an angle  $\beta_0$  relative to the grating normal at its pole. The grating will operate without aberration for a chosen object point and without linear field aberrations growing as the first power of the ruled width. The object and image fields are normal to the principal ray (the line connecting the grating pole with the object or image field center). This is simply the extension of our quasi-aplanatic

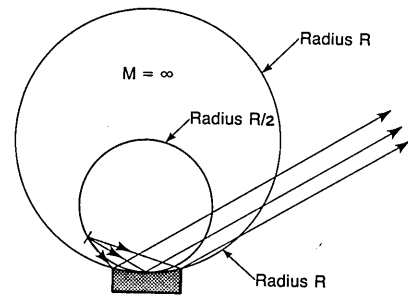


Fig. 10. Quasi-aplanatic grating with infinite magnification (a collimator). The source point lies along a circle with a diameter equal to the radius of grating curvature. A telescope ( $M = 0$ ) is obtained by reversing the direction of the rays.

grating to  $M = \infty$ . We note that the choice of beam direction is arbitrary and can be inverted to form a telescope rather than the collimator shown here.

The functional variation of the groove spacing obeys Eq. (2a). Applying the law of sines to Fig. 10, the following equations are obtained for the local angles of incidence and diffraction:

$$\alpha = \arctan[\sin\alpha_0 \cos(\Phi - \alpha_0) / [1 + \sin\alpha_0 \sin(\Phi - \alpha_0)]]; \quad (13a)$$

$$\beta = \beta_0 + \Phi. \quad (13b)$$

In Fig. 11(a) we plot the groove density as a function of the angular groove coordinate  $\Phi$  for the grating whose imaging properties were presented in Fig. 9. Such a grating requires at most only 2400 g/mm at the edge of the ruled width nearest the diffracted beam, which is consistent with the properly scaled results of Fig. 3. However, the groove density at the grating side nearest the object vanishes at a second point in addition to the zero groove density exhibited at the pole. This is due to the existence of two positions  $\Phi$  at which the incident and diffracted angles are equal. From Eqs. (13a) and (13b), one can show that this second position is at the angle  $\Phi$  for which

$$\tan\alpha_0 = \sin\Phi / (1 - \cos\Phi - 2\sin^2\Phi) \quad (14a)$$

or for small  $\Phi$

$$\Phi \approx -2 / (3 \tan\alpha_0). \quad (14b)$$

In the present example,  $\alpha_0 = 82^\circ$ , resulting in the observed zero point at  $\Phi = 0.094$ . On the basis of ruling density, the grating could extend over a numerical aperture of  $\sim 0.2$ , where the regions of groove density less than some minimum value (say 300 g/mm) are avoided during fabrication, or masked during use.

Optimal blazing of the desired wavelength is critical, as before, to provide comparable efficiency from all parts of the grating aperture. This requires that the illuminated groove facets be oriented symmetrically relative to the incident and diffracted directions, so as to obtain equal incident and diffracted angles relative to the facet normal. Relative to a plane tangent to the grating at its pole, the blaze angle orientation of the grooves should be

$$\tau(\Phi) = [\alpha(\Phi) - \beta(\Phi)] / 2 + \Phi. \quad (15)$$

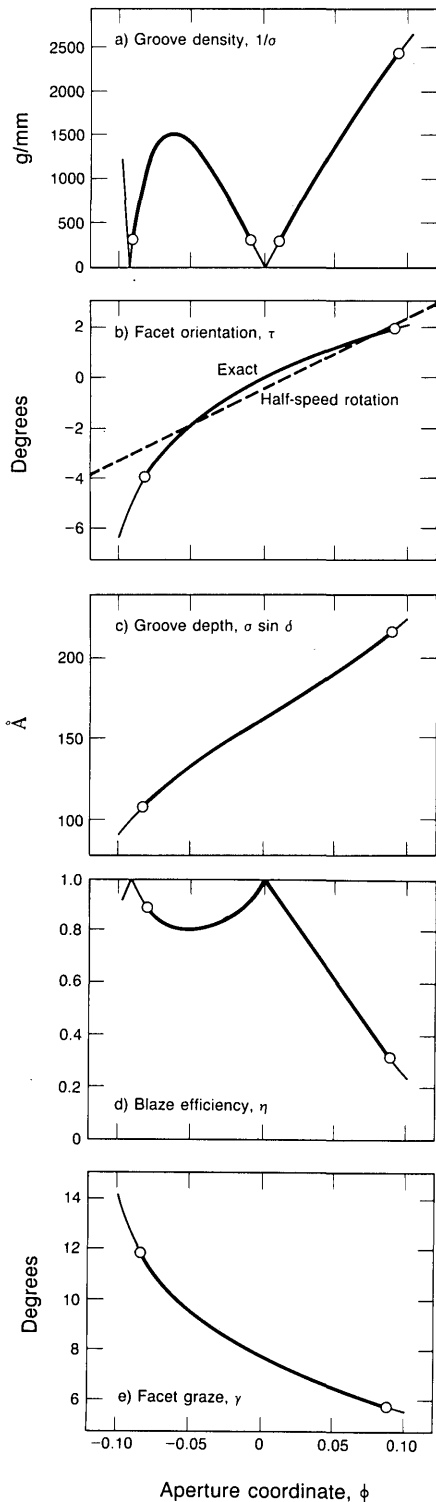


Fig. 11. Parameters for a quasi-aplanatic grating at infinite magnification vs the ruled aperture coordinate  $\Phi$ . The numerical aperture is equal to  $\Phi_{\max} - \Phi_{\min}$ . The grating radius is 50 mm, the wavelength is 45 Å, and the graze angle is 8°: (a) groove density vanishing at the two points where the angles of incidence and diffraction are equal; (b) groove facet orientation relative to the grating basal plane accompanied by a line showing the effect of an orientation which changes at half the rate of the surface slope; (c) depth of the groove assuming the blaze angle  $\delta$  varies according to the optimal value for  $\tau$  plotted in panel (b); (d) groove efficiency neglecting reflectance of the surface, showing the effect of shadowing when  $\alpha$  and  $\beta$  are unequal; (e) graze angle relative to the facet resulting in an increase in reflectance as the blaze efficiency decreases. The darkened sections of the curves in panels (a)–(e) indicate the usable aperture of the grating.

We plot in Fig. 11(b) these results for the same grating, showing a 6° variation in the facet orientation. A “half-speed” rotation, which was exact in the case of unit magnification, is a good approximation in the present case for numerical apertures  $a < 0.1$ .

The variation in groove depth is also a consideration. The depth  $D$  is simply equal to the local spacing times the sine of the local blaze angle,  $\delta(\Phi) = |\beta_0 - \alpha_0|/2$ .

This quantity was constant in the case of unit magnification, but Fig. 11(c) reveals a factor of 2 variation across the ruled width of our  $a = 0.2$  high magnification grating. This complicates the ruling, as it either requires comparable variation in the weight loading of the diamond tool<sup>14</sup> or can result in changes to the effective blazed wavelength.

In Fig. 11(d) is plotted the diffraction efficiency not including the reflectance of the coating. Assuming perfect blazing [Eq. (15)], this quantity is accurately derived from geometrical shadowing arguments<sup>40,41</sup> and is

$$\eta(\Phi) = \min(\cos\alpha/\cos\beta, \cos\beta/\cos\alpha). \quad (16)$$

This variation is almost a factor of 3 across a numerical aperture of  $a = 0.2$ . However, some relief is obtained when combined with the opposite trend in reflectance, which is due to the variation in graze angle plotted in Fig. 11(e). It is fortunate that the ratio in reflectance between opposite edges of the grating (6 and 12° graze angles) for 45 Å for a suitable coating (e.g., osmium) is  $\sim 30/10\% =$  factor of 3.<sup>22</sup> Thus, when combined with the variation shown in Fig. 11(d), the net absolute efficiency is expected to fluctuate by only 50%, which is acceptable on the basis of maintaining a diffraction width associated with the entire grating aperture.

Such a grazing incidence grating does not suffer from any fundamental design barriers down to spatial resolutions of 200 Å. Although we have used as an example a wavelength of 45 Å, we find the field of view to be relatively independent of the wavelength, providing the graze angle is linearly decreased to provide nearly the same reflectance. Of course, as discussed in Sec. II.B, both the groove density and required resolving power of the light decrease at shorter wavelengths. Thus, at 23 Å, a diffraction-limited spot size of 450 Å would require a numerical aperture of 0.05, be operated at a nominal graze angle of 4°, have a field of view as plotted in Fig. 9 for  $a = 0.10$ , and require a maximum groove density of 1600 g/mm and a linewidth corresponding to a resolving power of 1800.

#### IV. Two-Dimensional Imaging Systems

The analysis has so far been restricted to the plane of incidence and diffraction containing the grating ruled width. Given only this consideration, a point source would in general map onto a line focus, at the center of whose length the above results apply. Focusing in the perpendicular (sagittal) direction must also be provided to construct a point-to-point imaging system. In this section, we illustrate two ways in which such 2-D imaging can be obtained.

##### A. Single-Element Grating

The first-order aberration in the sagittal direction of a grating, i.e., along the lengths of its grooves, is astigmatism. Removal of this term requires the following well-known focusing condition:

$$1/r_0 - \cos\alpha_0/\rho + 1/r'_0 - \cos\beta_0/\rho = 0,$$

where we have assumed a general bicycle-tire toroid<sup>42</sup> with  $\rho$  being the radius of curvature in the direction of groove length. In the event of a centered grating,  $\beta_0 = \alpha_0$ , Eq. (16) reduces to the condition  $r_0 = \frac{1}{2}(1 + 1/M)\rho/\cos\alpha_0$ , where  $M$  is the magnification. For a spherical grating ( $\rho = R$ ), this is equivalent to Eq. (12b) for focusing in the ruled width direction if  $\alpha_0 = 45^\circ$ , independent of the magnification  $M$ . Such a mounting is illustrated in Fig. 12.

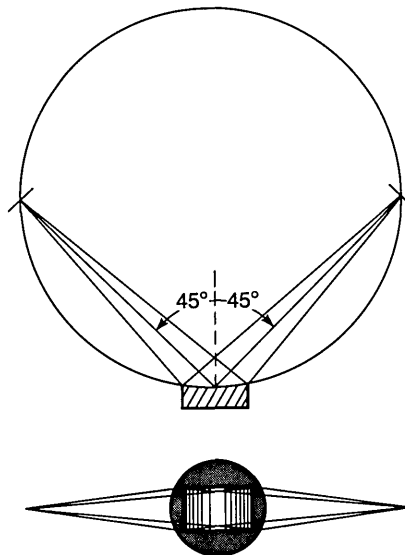


Fig. 12. Single spherical grating with straight grooves and 2-D imaging properties shown for unit magnification. The incidence and diffraction angle are 45°, resulting in the absence of both astigmatism and astigmatic coma. Aplanatism is obtained only in the plane of reflection (top panel), resulting in focal lines oriented normal to the principal ray, as shown.

Such a low incidence angle would not provide grazing incidence reflectivity and thus could not operate with conventional coatings at soft x-ray wavelengths. Independent of the reflectivity, the diffraction-limited resolution would be no smaller than  $\sim 0.1-0.2 \mu\text{m}$ , given a maximum groove density of 4800–6000 g/mm [see Eq. (2c)]. However, a unit magnification grating of this type would represent a simple submicron refocusing element which could operate efficiently at any wavelength longward of  $\sim 200 \text{ \AA}$ . Of course, aplanatic imaging holds only for a linear field or view within the plane of incidence.

With the removal of astigmatism, the next most dominant aberration not yet considered is sagittal (or astigmatic) coma, dependent on the mixed product  $wl^2$ , where  $w$  is the ruled width and  $l$  the groove length. Consistent with the notation of Eq. (5) for the aberration coefficients, we have<sup>42</sup>

$$F_{12} = -\frac{1}{2}(\sin\alpha_0/r_0)(1/r_0 - \cos\alpha_0/\rho) + \frac{1}{2}(\sin\beta_0/r'_0)(1/r'_0 - \cos\beta_0/\rho), \quad (17)$$

which also vanishes for the case  $\alpha_0 = \beta_0$  in unit magnification, independent of the radius of curvature. Naturally, application of Eq. 17 assumes that the choice of radius removes astigmatism.

##### B. Crossed Grating System

Point-to-point focusing at grazing incidence with a spherical grating requires a system of two such optics at orthogonal orientations, as in a Kirkpatrick-Baez mirror system.<sup>9</sup> As shown in Fig. 13, the upstream grating would provide a virtual line focus in the sagittal direction of the downstream grating and vice versa. For this geometry, we find that both Eqs. (16) and (17)

remain valid provided  $r_0$  is replaced by the distance  $s_0$  of the virtual sagittal focus from the downstream grating center and enters as a negative value in Eq. (16). Thus, for the case  $\beta_0 = \alpha_0$ , astigmatism is zero if

$$s_0 = (1/r'_0 - 2 \cos\alpha_0/\rho)^{-1}. \quad (18)$$

With this condition, the sagittal coma becomes

$$F_{12} = (\sin\alpha_0 \cos\alpha_0/\rho)(1/r'_0 - \cos\alpha_0/\rho). \quad (19)$$

For a spherical grating ( $\rho = R$ ), application of Eq. (4) for the transverse ray aberration yields the following image widths:

$$x_{12} = \frac{1}{2}a^2R \cos^2\alpha_0, M = 1; \quad (20a)$$

$$x_{12} = \frac{1}{8}a^2R \cos^2\alpha_0, M \ll 1; \quad (20b)$$

$$x_{12} = \frac{1}{8}a^2R \cos^3\alpha_0, M \gg 1. \quad (20c)$$

These values are non-negligible and limit the imaging performance of such a 2-D spherical grating system. For example, a unit magnification system with numerical aperture  $a = 0.05$ , a radius  $R = 50$  mm, and an incidence angle  $\alpha_0 = 82.0^\circ$  would have an aberration due to sagittal coma of  $\sim 1 \mu\text{m}$ . Thus very grazing angles of incidence are favored to obtain the highest spatial resolution.

Equal magnification in both directions can be obtained by a unit magnification system. The mid-point between the two gratings would coincide with the point  $\alpha_0 = \beta_0$  for either grating, the groove density increasing linearly toward the nearest focal point. In Fig. 14 we show the results of geometrical raytracing calculations of such a crossed grating system. Spherical gratings are used whose geometrical aberrations (dominantly sagittal coma as outlined above) limit the spatial resolution to  $\sim 0.2 \mu\text{m}$ . The field of view at this resolution was determined from raytracing to be  $\sim 20 \mu\text{m}$  in diameter, encompassing  $\sim 10,000$  2-D pixels. Each grating surface has a 50-mm radius and accepts a numerical aperture of 0.025. The groove density varies from  $\sim 600$  to  $\sim 1500$  g/mm over the 2.5-mm ruled width. Given 45-Å radiation, the diffraction-limited spot also contributes a FWHM of  $0.18 \mu\text{m}$  in both directions comparable to the geometrical aberrations shown in Fig. 14. Due to the small numerical aperture, these results could be obtained with a grating mechanically ruled in the conventional manner for which the blaze angle is oriented at a constant angle relative to some fixed plane.

In the event of cylindrical gratings, sagittal coma would be considerably smaller. On the basis of physical optics, a spatial resolution of  $0.09 \mu\text{m}$  could be obtained without requiring a variable blaze angle (see Sec. II.D). At a wavelength of 45 Å and an incidence angle of  $82^\circ$  this would require a maximum groove density of 1550 g/mm at the edges of a 5-mm ruled width (50-mm curvature radii) and incident light monochromatized to 1 part in 4000. The field of view would be  $\sim 10 \mu\text{m}$  in diameter (see Fig. 4) encompassing 10,000 2-D resolution elements. Of course, due to the absence of magnification in this or the previous spherical grating design, the imaging detector would need to

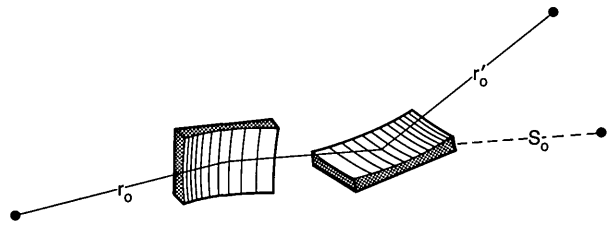


Fig. 13. Two-dimensional crossed system of spherical diffraction gratings with straight grooves. Aplanatism in 2-D and a wide imaging field is obtained if the magnification is unity, requiring symmetry about the mid-point between the gratings. This system has the same unit magnification in both directions (i.e., free of anamorphism). Nonunit magnification is also possible in the case of quasi-aplanatic spherical gratings.

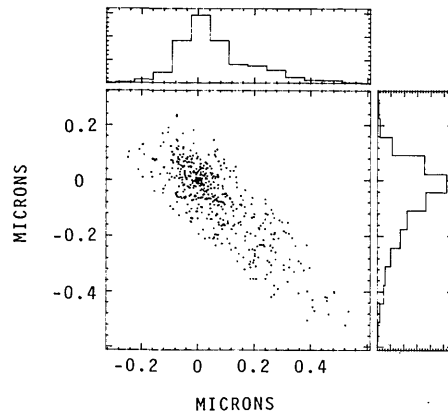


Fig. 14. Numerical raytracing of the spherical grating 2-D aplanatic grating system illustrated in Fig. 13. The angles of incidence and diffraction are  $84.0$  and  $88.0^\circ$ , the wavelength is  $45 \text{ \AA}$ , and the illuminated aperture is  $0.025 \times 0.025$ . A spatial resolution of  $\sim 0.2 \mu\text{m}$  is shown and maintained over a field of view  $20 \mu\text{m}$  in diameter encompassing  $\sim 10,000$  pixels. These results were obtained by use of the raytrace program SHADOW.

have a somewhat smaller pixel size than the detectable resolution of the object. This would require the use of a high-resolution resist such as polymethylmethacrylate (PMMA).<sup>43</sup>

At large magnification, Eq. (20c) reveals that sagittal coma for a spherical grating is small. This residual could be removed by use of slightly curved grooves using the mechanical ruling techniques demonstrated by Harada and Kita<sup>10</sup> and by Hirst.<sup>14</sup> However, Eqs. (20b) and (20c) assume a real source, and thus the direction of the optical path must be reversed to compute the aberration for the downstream grating. Therefore, although  $M \gg 1$  for the first grating, a value  $M \ll 1$  must be used for the second grating, and thus Eq. (20b) must be applied. This yields a considerably higher aberration (factor of  $1/\cos\alpha_0$ ), which would require an unfeasible amount of groove curvature to remove.

The ideal grating surface for nonunit magnification would be a cylinder ( $\rho_0 = \infty$ ). The grating could be

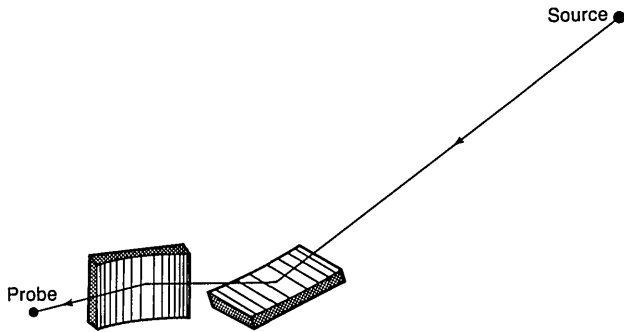


Fig. 15. Cylindrical grating microprobe at high demagnification. Quasi-aplanatic 2-D focusing is obtained without the aberration of sagittal coma. The radius of curvature and demagnification differ for the two gratings. Minimum monochromaticity of the incident light is required if the incidence and diffraction angles are equal at the center of each grating. At small graze angles, spherical gratings can be substituted for the cylindrical gratings shown.

ruled in the conventional manner, with straight and parallel grooves formed at the intersection of ruling planes normal to the surface at its center. Such a grating would have its virtual focal distance  $s_0$  equal to the image distance  $r'_0$ , which has been previously discussed in the case of a plane grating for spectroscopy.<sup>11</sup> In the present nonspectroscopic application, we can set  $\beta_0 = \alpha_0$  at the grating center and thereby remove sagittal coma. The effect of higher-order mixed terms in the aberration function remains an issue for further investigation.

The ultimate system on the basis of attainable spatial resolution is pictured in Fig. 15. It combines 2-D focusing with high demagnifications (300 in one direction; 150 in the other) and large numerical apertures (0.2 for one grating; 0.1 for the other). As shown in Fig. 9, the gratings will individually provide resolutions from 300 to 600 Å. This system would function as a microprobe whose light source must be 10 μm (or smaller) in diameter and monochromatized to 1 part in 5000 at a wavelength of 45 Å (or 1 part in 2500 at a wavelength of 23 Å). The required groove densities would be 2400 g/mm (or 1200 g/mm) for the first grating and 1200 g/mm (or 600 g/mm) for the second grating. The distance to the light source would be ~2 m. This system would be an ideal imaging device for use as a scanning microprobe/microscope.

### C. Normal Incidence

It is a well known fact that normal incidence optics deliver wider fields of view than those at grazing incidence. The same is true of an aplanatic grating. From Eq. (12), we see that in the limit as the angles of incidence and diffraction vanish, quasi-aplanatic solutions are obtained independent of the radius of curvature. This result has been used in practice to develop normal incidence transmission flat zone plates with usable fields of view for imaging.<sup>1,19-22</sup> Due to the axisymmetric nature of normal incidence, circular grooves or zones provide complete 2-D imaging in a single optic.

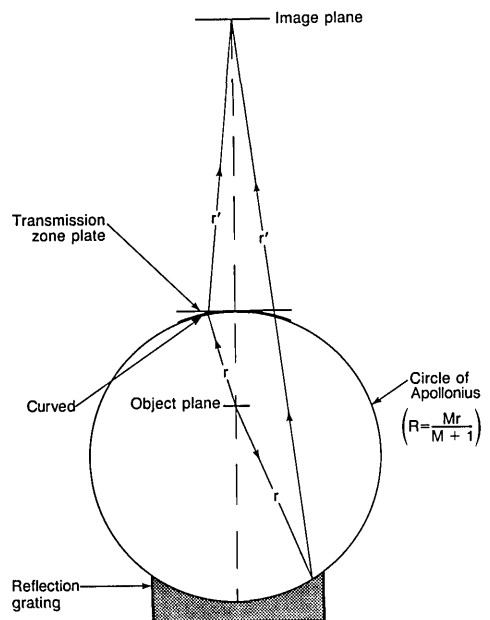


Fig. 16. Normal incidence spherical zone plate proposed by Murty. The circle of Apollonius harmonically divides the distance between object and image, resulting in an equal ratio  $r'/r$  over the spherical aperture. There is a fortuitous cancellation of the effects of grating magnification and obliquity of field away from the axis of symmetry, leading to a higher level of aplanatism than is associated with the classical sine rule. The grooves are circles rotated around the symmetry axis, and the spherical zone plate can theoretically be used in reflection or transmission.

However, the flat zone plate is not completely aplanatic. The dominant field aberration is linear with off-axis angle, and depends on the second power of the numerical aperture [derivable from Eqs. (5) or Ref. 20].

$$\Delta x(\text{geometrical}) = 3/8 \times a^2 \quad (21)$$

Taking the optimum case  $\Delta x(\text{geometrical}) = \Delta x_d$  (physical diffraction limit), then  $a = \lambda_*/\Delta x$ , and the largest off-axis angle which can be used at this resolution is  $x = 8/3 \Delta x^3/\lambda_*^2$ . This yields the total field of view of:

$$\text{FOV} = 16/3 \Delta x^2/\lambda_*^2 \text{ pixels} \quad (22)$$

in each two dimensions. For example, at a wavelength of 45 Å, there are approximately 10,000 one-dimensional pixels available for imaging at a resolution of 0.2 μm, but only 240 pixels for such a zone plate whose physical optics limit is 300 Å resolution. To obtain useful fields of view at resolutions below approximately 0.1 μm, it is therefore necessary to consider a more nearly aplanatic optical surface.

In 1960 Murty proposed such an aplanatic normal incidence zone plate diffraction grating in reflection or transmission.<sup>44</sup> By using the sine condition for a mirror, he arrived at a spherical grating surface equal to the circle of Apollonius (Fig. 6). This surface does not pass through either the image or object points and, therefore, is not simply the normal incidence limit of the grazing incidence gratings presented above.

Nonetheless, application of our general grating magnification factor [Eq. (1)] can be shown to retrieve the solution proposed by Murty. However, we note that since one is removing ray aberration terms which depend on second and higher powers of the aperture, both the effect of grating magnification ( $\cos\alpha/\cos\beta$ ) and focal surface obliquity ( $\cos\theta/\cos\theta'$ ) must be considered. To a high degree of accuracy, these two terms cancel at normal incidence, and one (fortuitously) retains only the sine rule factor ( $r'/r$ ) assumed by Murty for this diffraction grating. As the obliquity factor holds for any optic (grating or mirror), this cancellation leads to an exactness of the classical sine rule not present in the case of a mirror. Of course, at non-normal incidence, this simplification does not occur; in the case of grazing incidence, the grating magnification factor is comparable to the factor  $r'/r$ , which allowed us to obtain the aplanatic and quasi-aplanatic solutions presented above.

The curvature radius for the normal incidence aplanatic grating of Murty is

$$R = rM/(M + 1), \quad (23)$$

which provides for both convex surfaces in transmission and concave surfaces in reflection. Interestingly, the required groove density is equal to that (two adjacent zones) of a zone plate. Thus, this optic would have the same practical limitation of requiring an outer zone (or groove) width comparable to the spatial resolution from physical optics.

Using Eqs. (5), we found that an aplanatic normal incidence zone plate (or reflection grating) would have a field of view of 5000 pixels at a resolution of 300 Å. This represents a factor of 20 improvement over a flat zone plate, permitting simultaneous imaging of objects extending over 100 μm. However, the width of the outer zone would have to be 300 Å, corresponding to a groove density of ~16,500 g/mm. At high magnification, we have  $R \approx r = D/a$ , where  $D$  is the grating aperture size. With  $D = 100 \mu\text{m}$ , such as provided by electron lithography,<sup>22</sup> and  $a = 0.1$ , the required radius of curvature is ~1 mm.

## V. Conclusions

An imaging grating of the type introduced here has obvious applicability to soft x-ray microscopy in the biological and materials sciences. For spatial resolutions above 0.1 μm, such a grating can be fabricated using current technology. The required metrological accuracy in the placement of grating grooves is no better than that of a nonimaging grating of the same groove density at the required spectral resolution. By use of a small curvature radius, spectral resolutions are typically a few ×1000.

Below ~0.1 μm, an enhancement in existing ruling engines will be required, allowing a variation in the blaze angle relative to a fixed plane while maintaining a spectral resolution limited by the entire ruled width. Such a grating could reach spatial resolutions of ~200 Å. It is also possible to employ other fabrication methods, such as visible/UV holography.<sup>20,45</sup> In a fol-

lowing paper, we will report on detailed 3-D ray trace simulations and aberration analysis of a soft x-ray microscope based on the concepts presented here.

The author thanks F. Cerrina for providing him with the ray tracing program SHADOW and modifications to accommodate varied-space gratings, and acknowledges helpful discussions with J. H. Underwood. This work was supported by the U.S. Department of Energy under contract DE-AC03-76SF00098.

## References

1. G. Schmahl, B. Niermann, D. Rudolf, P. Guttman, and V. Sarafis, "X-ray Microscopy: Experimental Results with the Göttingen X-Ray Microscope at the Electron Storage Ring BESSY in Berlin," *J. Microsc.* **138**, 279 (1985). For a review of the scientific potential in biological soft x-ray microscopy, see J. Kirz and D. Sayre, "Soft X-ray Microscopy of Biological Specimens," in *Synchrotron Radiation Research*, H. Winnick, Ed. (Plenum, New York, 1980), p. 277.
2. D. T. Attwood, "Diagnostics for the Laser Fusion Program—Plasma Physics on the Scale of Microns and Picoseconds," *IEEE J. Quantum Electron.* **QE-14-12**, 909 (1978).
3. E. Spiller and R. Feder, "X-ray Lithography," in *X-ray Optics: Applications to Solids*, H.-J. Queisser, Ed. (Springer-Verlag, Berlin, 1977), p. 35; A. R. Neureuther, "Microlithography with Soft X-rays," in *Synchrotron Radiation Research*, H. Winnick, Ed. (Plenum, New York, 1980), p. 223.
4. F. Cerrina, "X-ray Imaging with Synchrotron Radiation," *J. Imag. Sci.*, in press (1986).
5. R.-P. Haelbich, "A Scanning Ultrasoft X-ray Microscope with Multilayer Coated Reflection Optics: First Test with Synchrotron Radiation Around 50 eV Photon Energy," in *Scanned Image Microscopy*, E. A. Ash, Ed. (Academic, London, 1980), p. 413.
6. H. Wolter, "Grazing Incidence Mirror Systems for X-rays," *Ann. Phys.* **10**, 94 (1952); "Generalized Schwarzschild Systems of Mirrors with Glancing Reflection as Optical Systems for X-rays," *Ann. Phys.* **10**, 286 (1952).
7. J. K. Silk, "A Grazing Incidence Microscope for X-ray Imaging Applications," in *Ultrasoft X-ray-Microscopy: Its Applications to Biological and Physical Sciences*, D. F. Parsons, Ed. (Ann. NY Acad. Sci.) **342**, 116 (1980).
8. A. Franks and M. Stedman, "Reflection X-ray Microscopy," *J. Microsc.* **138**, 237 (1985).
9. P. Kirkpatrick and A. V. Baez, "Formation of Optical Images by X-rays," *J. Opt. Soc. Am.* **38**, 766 (1948).
10. T. Harada and T. Kita, "Mechanically Ruled Aberration-Corrected Concave Gratings," *Appl. Opt.* **19**, 3987 (1980).
11. M. C. Hettrick and S. Bowyer, "Variable Line-Space Gratings: New Designs for Use in Grazing Incidence Spectrometers," *Appl. Opt.* **22**, 3921 (1983).
12. T. Harada, M. Itou, and T. Kita, "A Grazing Incidence Monochromator with a Varied Space Plane Grating for Synchrotron Radiation," *Proc. Soc. Photo-Opt. Instrum. Eng.* **503**, 114 (1984).
13. M. C. Hettrick, S. Bowyer, R. Malina, C. Martin, and S. Mrowka, "Extreme Ultraviolet Explorer Spectrometer," *Appl. Opt.* **24**, 1737 (1985).
14. G. E. Hirst, "Some Recent Developments in the Fabrication of Variably-Spaced Linear and Circular Diffraction Gratings," *Proc. Soc. Photo-Opt. Instrum. Eng.* **560**, 64 (1985).
15. T. Kita, T. Harada, N. Nakano, and H. Kuroda, "Mechanically Ruled Aberration-corrected Concave Gratings for a Flat-field Grazing Incidence Spectrometer," *Appl. Opt.* **22**, 512 (1983).
16. M. C. Hettrick, S. M. Kahn, W. Craig, and R. Falcone, "Stigmatic Grazing Incidence Laboratory Plasma Spectrometer with

- Variable Line-Space Grating," in preparation.
17. See any textbook on geometrical optics; e.g., M. Born and E. Wolf, *Principles of Optics* (Pergamon, New York, 1980), p. 167.
  18. The sine condition is in fact only an approximation accurate for small numerical apertures. As the aperture is widened, rays will impinge on the focal plane at oblique angles and thus cause increases in linear magnification in the event of an off-axis source. However, if the central ray hits the focal plane at normal incidence, this effect will scale only as the cosine of the numerical aperture. For other proposed modifications to the classical sine rule for a mirror, see the following: R. A. M. Keski-Kuha, "A Modified Sine-condition for Single Reflection X-ray Optics," Ph.D. dissertation, Saint Louis U. (1982); T. T. Saha, "Abbe's Sine-condition and a Modified Sine-condition for Two-reflector X-ray Optics," Ph.D. dissertation, Saint Louis U. (1982).
  19. J. L. Soret, *Ann. Phys. Chem.* **156**, 99 (1875).
  20. A more recent discussion is given by D. Rudolph and G. Schmahl, "High Power Zone Plates for a Soft X-ray Microscope," *Ann. NY Acad. Sci.* **342**, 94 (1980).
  21. G. Schmahl, D. Rudolph, P. Guttman, and O. Christ, "Zone Plates for X-ray Microscopy," in *X-ray Microscopy*, G. Schmahl and D. Rudolph, Eds. (Springer-Verlag, Göttingen, 1983), p. 63.
  22. D. Kern *et al.*, "Electron Beam Fabrication and Characterization of Fresnel Zone Plates for Soft X-ray Microscopy," *Proc. Soc. Photo-Opt. Instrum. Eng.* **447**, 204 (1983).
  23. B. L. Henke, P. Lee, T. J. Tanaka, R. L. Shimabukuro, and B. K. Fujikawa, "Low-energy X-ray Interaction Coefficients: Photoabsorption, Scattering and Reflection," *At. Nucl. Data Tables* **27**, 1 (1982).
  24. B. Lai, F. Cerrina, and M. Pouey, "Extreme UV Circle Spectrometer for Line Profile Measurements," in *Proceedings, AIP Conference on Short Wavelength Coherent Radiation* (Monterey, 1986).
  25. M. C. Hettrick and J. H. Underwood, "Varied-Space Grazing Incidence Gratings in High Resolution Scanning Spectrometers," in *Proceedings, AIP Conference on Short Wavelength Coherent Radiation* (Monterey, 1986).
  26. D. Attwood, K. Halbach, and K.-J. Kim, "Tunable Coherent X-rays," *Science* **228**, 1265 (1985).
  27. H. G. Beutler, "The Theory of the Concave Grating," *J. Opt. Soc. Am.* **35**, 311 (1945).
  28. T. Namioka, "Theory of the Concave Grating. I," *J. Opt. Soc. Am.* **49**, 446 (1959).
  29. Ray tracings were made using the program described in B. Lai and F. Cerrina, "SHADOW: A Synchrotron Radiation Ray Tracing Program," *Nucl. Instrum. Meth.* **A246**, 337 (1986).
  30. M. Neviere and W. R. Hunter, "Analysis of the Changes in Efficiency Across the Ruled Area of a Concave Diffraction Grating," *Appl. Opt.* **19**, 2059 (1980).
  31. M. C. Hutley and W. R. Hunter, "Variation of Blaze of Concave Diffraction Gratings," *Appl. Opt.* **20**, 245 (1981).
  32. T. Kita and T. Harada, "Use of Aberration-Corrected Concave Gratings in Optical Demultiplexers," *Appl. Opt.* **22**, 819 (1983).
  33. B. Niemann, "Detective Quantum Efficiency of Some Film Materials in the Soft X-ray Region," *Ann. NY Acad. Sci.* **342**, 230 (1980).
  34. B. L. Henke, S. L. Kwok, J. Y. Ueijo, H. T. Yamada, and G. C. Young, "Low-energy X-ray Response of Photographic Films, I. Mathematical Models," *J. Opt. Soc. Am. B* **1**, 818 (1984); B. L. Henke, F. J. Fujiwara, M. A. Tester, C. H. Dittmore, and M. A. Palmer, "II. Experimental Characterization," *J. Opt. Soc. Am. B* **1**, 828 (1984).
  35. J. P. Henry, E. M. Kellogg, U. G. Briel, S. S. Murray, and L. P. Van Speybroeck, "High Resolution Imaging X-ray Detector for Astronomical Measurements," *Proc. Soc. Photo-Opt. Instrum. Eng.* **106**, 196 (1977); for a recent review, see O. H. W. Siegmund and R. F. Malina, "Detection of Extreme UV and Soft X-rays with Microchannel Plates: A Review," in *Multichannel Image Detectors, Vol. 2*, Y. Talmi, Ed. (American Chemical Society, Washington, DC, 1983), p. 253.
  36. A. Franks, B. Gale, K. Lindsey, D. J. Pugh, C. J. Robbie, and M. Stedman, "Optical Components for X-ray Microscopy," *Ann. NY Acad. Sci.* **342**, 167 (1980).
  37. H. Rarback *et al.*, "Recent Results from the Stony Brook Scanning Microscope," in *X-ray Microscopy*, G. Schmahl and D. Rudolph, Eds. (Springer-Verlag, Göttingen, 1983), p. 203.
  38. H. Rarback and J. Kirz, "Optical Performance of Apodized Zone-Plates," *Proc. Soc. Photo-Opt. Instrum. Eng.* **316**, 120 (1981).
  39. J. F. Meekins, R. G. Cruddace, and H. Gursky, "Diffraction Limitations of a High-Resolution Spectrometer Coupled to a Wolter Telescope," *Appl. Opt.* **24**, 2872 (1985).
  40. D. Maystre and R. Petit, "Quelques Récents Résultats en Théorie des Réseaux; Application a Leur Utilisation dans l'Extrême Ultraviolet," *Nouv. Rev. Opt.* **7**, 165 (1976).
  41. M. Neviere, D. Maystre, and W. R. Hunter, "On the Use of Classical and Conical Diffraction Mountings for XUV Gratings," *J. Opt. Soc. Am.* **68**, 1106 (1978).
  42. H. Haber, "The Torus Grating," *J. Opt. Soc. Am.* **40**, 153 (1950).
  43. G. N. Taylor, "X-ray Resist Materials," *Solid State Technol.* (May 1980), p. 73.
  44. M. V. R. K. Murty, "Spherical Zone-Plate Diffraction Grating," *J. Opt. Soc. Am.* **50**, 932 (1960).
  45. M. C. Hutley, "Diffraction Gratings," in *Techniques of Physics, Vol. 4* (Academic, New York, 1982), p. 99.